RESEARCH   **Open Access**

Tumor segmentation in brain MRI using a fuzzy approach with class center priors

Moumen T El-Melegy[1*] and Hashim M Mokhtar[2]

Abstract

This paper proposes a new fuzzy approach for the automatic segmentation of normal and pathological brain magnetic resonance imaging (MRI) volumetric datasets. The proposed approach reformulates the popular fuzzy c-means (FCM) algorithm to take into account any available information about the class center. The uncertainty in this information is also modeled. This information serves to regularize the clusters produced by the FCM algorithm thus boosting its performance under noisy and unexpected data acquisition conditions. In addition, it also speeds up the convergence process of the algorithm. Experiments using simulated and real, both normal and pathological, MRI volumes of the human brain show that the proposed approach has considerable better segmentation accuracy, robustness against noise, and faster response compared with several well-known fuzzy and non-fuzzy techniques reported in the literature.

Keywords: Prior information; MRI segmentation; Fuzzy c-means; Fuzzy algorithms; Brain MRI; Tumor segmentation

1 Introduction

Magnetic resonance imaging (MRI) of the brain is often used to monitor tumor response to treatment process. The segmentation of the brain tumor from the magnetic resonance images is important in medical diagnosis because it provides information associated to anatomical structures as well as potential abnormal tissues necessary to treatment planning and patient follow-up. It can also be helpful for general modeling of pathological brains and the construction of pathological brain atlases [1]. One example is to analyze and estimate quantitatively the growth process of brain tumors, and to assess the response to treatment and in guiding appropriate therapy in serial studies [2,3]. In spite of numerous efforts and promising results in the medical imaging community, accurate and reproducible segmentation and characterization of abnormalities are still a challenging and difficult task because of the variety of the possible shapes, locations and image intensities of various types of tumors. This task involves various disciplines including medicine, MRI physic, radiologist's perception, and image analysis based on intensity and shape.

Brain tumor segmentation process consists of separating the different tumor tissues, such as solid tumor, edema, and necrosis from the normal brain tissues, such as gray matter (GM), white matter (WM), and cerebrospinal fluid (CSF). Although manual segmentation by qualified professionals remains superior in quality to automatic methods, it has two drawbacks. The first drawback is that producing manual segmentations or semi-automatic segmentations is extremely time-consuming, with higher accuracies on more finely detailed volumes demanding increased time from medical experts. The second problem with manual and semiautomatic segmentations is that the segmentation is subject to variations both between observers and within the same observer. For example, a study by Mazzara et al. [1] quantified an average of 28% ± 12% variation in quantified volume between individuals performing the same brain tumor segmentation task, and quantified a 20% ± 15% variation within individuals repeating the task three times at one month intervals. This statistic demonstrates that the manual segmentation has no confidence in tracking the tumor volume during the patient follow-up process and the automatic methods that could achieve a sufficient level of accuracy would be highly desirable for their ability to perform high-throughput segmentation. On the other hand, automatic methods would be advantageous since they are not subject to this variation, and thus,

* Correspondence: moumen@aun.edu.eg
[1]Electrical Engineering Department, Assiut University, Assiut 71516, Egypt
Full list of author information is available at the end of the article

the significance of changes in volumes could be more easily assessed.

In addition to tumor volume calculation, accurate automatic segmentation methods additionally have the potential to reduce the variability and increase the standardization of other measurements and protocols, including the quantification of edema or necrosis. Also, automatic segmentation could lead to new applications, including effective content-based image retrieval in large medical databases. This could allow clinicians to find similar images in historical data based on tumor location, grade, size, enhancement, extent of edema, similar patterns of growth, or a variety of other factors. This information could help clinicians in making decisions, in addition to being a useful research tool for exploring patterns in the historical data. In a similar vein, accurate high-throughput segmentations could be used in combination with relevant features and machine learning methods to improve tumor grading in cases where grading is ambivalent (or to discover potentially useful distinctions within grades), and to provide a more accurate and patient-specific prognosis [4].

Due to the above advantages of the automatic segmentation, it becomes a necessary issue for clinicians. Nevertheless, automatic tumor segmentation is still a difficult problem for two key reasons: (1) There is a large number of tumor types which differ greatly in size, shape, location, tissue composition and tissue homogeneity [5]. In some cases, their border with normal tissues cannot be very well defined on images; therefore, they are even difficult for radiology experts to delineate. (2) The consequence of the phenomenon of partial volume effect (PVE), where 1 pixel/voxel may belong to multiple tissue types, in addition to noise due to the MRI acquisition system.

In this paper, we address these difficulties using a soft computing approach based on fuzzy concepts. This fuzzy approach provides several advantages. First, it inherently has the attractive property of the soft classification model, where each point can belong to more than one class. This is consistent with the partial volume effect observed in MR images and thus eliminates the need for explicit modeling of mixed classes (which is required - for example - by segmentation methods based on the finite Gaussian mixture [5]). Another key advantage of the fuzzy approach is that it can segment several tissues at the same time. Therefore, this approach can be used to segment all brain tissues of interest, such as tumor and other abnormal tissues (e.g., edema and necrosis) in addition to the normal brain tissues (e.g., WM, GM, and CSF). This is in contrast to some popular methods for medical image segmentation, such as deformable models [6,7] and level sets [8,9], where only one object or tissue of interest can be typically segmented at any time. Moreover, while these latter segmentation methods often need careful (sometimes even manual) close-enough initialization to ensure the method

convergence to a proper solution, the proposed approach can start with random initial values.

In particular, the fuzzy approach that we propose is based on the fuzzy c-means (FCM) algorithm [10,11]. Indeed, this fuzzy clustering algorithm has been already used for MRI segmentation (e.g., Ahmed et al. [12], Caldairou et al. [13], Cai et al. [14]). One key contribution of this paper is that the proposed approach, unlike the earlier ones, is able to utilize prior information in the segmentation process. It incorporates available information about the class centers of the data. This can be as simple as the rough knowledge of the mean intensity (class center in FCM terminology) of a class (a particular tissue in the MRI data). The uncertainty in this information is also modeled. This information serves to regularize the clusters produced by the FCM algorithm thus boosting its performance under noisy and unexpected data acquisition conditions. In addition, it speeds up the convergence process of the algorithm. To the best of our knowledge, the idea, mathematical formulation, and derivation of incorporating this information have not been reported before in the wide literature of fuzzy clustering and its applications.

We apply the proposed approach to the automatic segmentation of the human brain from two popular benchmark MR datasets: the simulated BrainWeb MR datasets [15], and normal real MR datasets obtained from the Internet Brain Segmentation Repository (IBSR) [16]. We compare these results with those of the standard FCM and several well-known fuzzy and non-fuzzy MRI segmentation techniques found in the literature. We also apply the proposed approach to pathological T1-weighted MRI databases obtained from IBSR and from a local MRI scan center to detect hyper-intense tumors. The results on the pathological MRI are evaluated by expert radiologists from Assiut University Medical Hospital.

The remainder of this paper is organized as follows: Section 2 briefly reviews related work. Section 3 gives a concise description of the standard FCM algorithm. In section 4, a full explanation of the proposed approach for MRI segmentation is given. Our approach for tumor segmentation is developed in section 5. Section 6 presents the experimental results and some comparisons with other methods. Finally, the paper is concluded in section 7.

2 Related work

Many techniques for MRI segmentation have been developed over the years based on several techniques. These techniques can be divided into four major classes [17]: threshold-based techniques, region-based techniques, pixel classification techniques, and model-based techniques. In this section, we give a brief overview on these methods. The interested reader is referred to the recent survey in [17] for more details.

One of the earliest and classical methods is thresholding, in which the objects of the image are classified by comparing their intensities with one or more intensity thresholds. These thresholds can be either global or local. For example, Gibbs et al. [18] presented a semi-supervised approach for the segmentation of enhancing tumor pixels from T1-weighted post-contrast images. It first applied an intensity threshold to a manually selected region of interest, and represents a clearly justified approach for segmenting image objects that are different in intensity from their surroundings. Their method does not effectively take into account the presence of hyper-intense pixels representing normal structures in T1 post-contrast images. Other segmentation methods based on thresholding include those in [19,20]. However, generally threshold-based segmentation methods, either local or global, are unable to exploit all the information provided by MRI and are often used as a first step in the segmentation process.

Region-based segmentation approaches (e.g. [21-23]) examine pixels in an image and form disjoint regions by merging neighborhood pixels with homogeneity properties based on a predefined similarity criterion. One example is the work of Salman [21] who presented a comparative analysis of the traditional region growing segmentation and a modified region growing method, addressed to brain tumor segmentation in 3D T1 MR images. Other approaches incorporate the region growing process as a refinement step [22] or in an adaptive fashion [23]. While the advantage of region growing is its capability of correctly segmenting regions that have similar properties and generating connected region, it suffers from the partial volume effect which limits the accuracy of MR brain image segmentation. Partial volume effect blurs the intensity distinction between tissue classes at the border of the two tissues types, because the voxel may represent more than one kind of tissue types.

In brain tumor segmentation, the methods based on pixel classification are constrained to the use of supervised or unsupervised classifiers to cluster pixels in the feature space. While the supervised methods include Bayes classifiers and artificial neural networks, unsupervised methods include k-means, fuzzy clustering techniques [10,11], and statistical methods such as Markov random fields (MRF). Fuzzy methods will be discussed in more detail later in this section. The unsupervised method of MRF provides a way to integrate spatial information into the clustering process, reducing the overlapping of clusters and the effect of noise on the result [24]. A major difficulty in MRF is the selection of the parameters that control the strength of spatial interactions, which can result in very soft segmentation and a loss of structural details.

In model-based segmentation, a connected and continuous model is built for a specific anatomic structure by incorporating *a priori* knowledge of the object such

as shape, location, and orientation. The key methods in this class often employ active contour models or snakes [6,7] and level set methods [8,9]. While the former generally suffers from the difficulty of naturally handling topological changes for the splitting and merging of contours, level set handles this in a natural fashion. Segmenting tumors by geometric deformable models or level sets permits the development of fully automatic and highly accurate segmentation approaches [17]. Unfortunately, these methods are still computationally expensive [9,17], and sometimes hard to initialize [8].

One of the clustering algorithms that have enjoyed considerable success in image clustering and segmentation is the well-known FCM [10,11] and its variants. This fuzzy approach provides several advantages. First, it inherently offers a soft classification model, which is consistent with the partial volume effect observed in MR images and thus eliminates the need for explicit modeling of mixed classes (which is required - for example - by segmentation methods based on the finite Gaussian mixture [5]). Another key advantage of the fuzzy approach is that it can segment several tissues at the same time. Therefore, this approach can be used to segment all brain tissues of interest, such as tumor and other abnormal tissues (e.g., edema and necrosis) in addition to the normal brain tissues (e.g., WM, GM, and CSF). This is in contrast to deformable models [6,7] and level sets [8,9], where only one object or tissue of interest can be typically segmented at any time.

A lot of work has been developed in order to further improve the FCM performance for MRI segmentation. Almost all these efforts have focused on imposing spatial constraints into the clustering algorithm [12-14,25-29]. Some notable examples of these methods follow.

Liew et al. [25] proposed a fuzzy algorithm that incorporates the local spatial context. Kang et al. [30] improved FCM with adaptive weighted average filter. Ahmed et al. [12] modified the objective function of FCM to allow the labeling of a pixel to be influenced by the labels in its immediate neighborhood. But the main disadvantage is that it computes the neighborhood term in each iteration step, which is time-consuming. Chen and Zhang [27] proposed two variant algorithms, which simplified the neighborhood term of the objective function of [12]. Chuang et al. [28] proposed averaging the fuzzy membership function values and reassigning them according to a tradeoff between the original and averaged membership values. This approach can produce accurate clustering if the tradeoff is well adjusted empirically, but it is enormously time-consuming. Cai et al. [14] proposed a fast generalized FCM algorithm which incorporates the spatial information, the intensity of the local pixel neighborhood and the number of gray levels in an image. This algorithm forms a nonlinearly

weighted sum image from both original image and its local spatial and gray level neighborhood.

Hoppner and Klawonn [31] introduced a new way to constrain the membership functions and proposed a FCM-based algorithm with improved fuzzy partitions. They modified the objective function so that the FCM algorithm worked on distances to the Voronoi cell of the cluster rather than using distances to the cluster prototypes. Zhu et al. [32] improved on the algorithm of [31] and proposed a generalized FCM clustering algorithm with the fuzziness index being set by the users so as to achieve more effective clustering performance. Both the algorithms of [31] and [32] rewarded the crisp membership degrees and made the FCM-based algorithm faster with fewer iteration steps. Unfortunately, this kind of method makes FCM lose its attractive soft classification nature rendering it no longer suitable to take PVE into account.

Ji et al. [33] constructed a regular energy term to deal with the effect of noise by using the non-local patch information. This method needs to choose different parameters of the regular energy term when segmenting different images. More recently, along the same line, the fuzzy local [28] and non-local [13,22,34] information c-means algorithms have been proposed.

The previous methods have been developed for image and/or MRI segmentation. There are several methods that are crafted for the particular sake of tumor segmentation from MRI, including level sets [8,9], expectation-maximization algorithm [17,35] and fuzzy techniques [33,36-38].

The above methods for normal and/or pathological MRI segmentation have some known limitations. On the one hand, the majority of them has focused on imposing some sort of spatial constraints over a local neighborhood, and requires a tunable parameter to weigh the importance of these constraints relative to the data-driven objective function. This parameter has a crucial impact on the performance of those methods, and its selection is generally difficult and needs some trial-and-error experiments. Some few methods (e.g. [13]) have however tried to get around this problem by making the determination of this parameter adaptive and data-dependent. On the other hand, some of these methods (e.g. [33]) need user intervention one way or the other.

The approach proposed in this paper goes around these issues by following a different, novel methodology. The approach makes use of available information about the mean intensities of the various MR tissues and their uncertainty to guide the minimization of the data-driven objective function. Such prior information can be easily extracted from some training MRI samples of these tissues. The incorporation of this information allows the automatic segmentation of these tissues from the MRI datasets, without the need for any parameters or weighting factors to be tuned. This also enhances the approach performance in terms of accuracy, noise robustness and speed, as will be demonstrated in our experimental results.

3 Standard FCM

In this section, we give a brief overview of the standard FCM clustering algorithm. It was first introduced by Dunn [10] and later extended by Bezdek [11]. Its objective is to partition data in such a way that the data points within one cluster are as similar to each as possible and as far away as it can be from the data points of other clusters. In the context of our work, the FCM approach can be formulated as follows. Let us consider an image (or MRI data volume) composed of a set of N points (voxels). Let us suppose that this volume has to be segmented into K ($K \geq 2$) classes, in a fuzzy fashion. This means that a point i does not necessarily belong to one of the K classes, but can partially belong to several ones. For each point $i \in N$, let $(u_{ic})_{c=1}^{K} = (u_{i1}, u_{i2}, \ldots\ldots, u_{iK})$ be the memberships of the point i with respect to these K classes, such that $\sum_{c=1}^{K} u_{ic} = 1$ and $u_{ic} \in [0, 1]$. For each class c let v_c be the centroid (class center) of this class (this usually corresponds to the mean value of this class's points). In the FCM approach, the segmentation process of the image (volume) can be defined as the minimization of the energy function

$$J_{\text{FCM}} = \sum_{c=1}^{K} \sum_{i=1}^{N} u_{ic}^{m} \| y_i - v_c \|^2. \tag{1}$$

The parameter m is a weighting exponent on each fuzzy membership and determines the amount of fuzziness of the resulting classification (typically set to 2). This function in (1) can be easily minimized using the Lagrange multiplier (λ), so the constrained optimization becomes

$$F_{\text{FCM}} = \sum_{c=1}^{K} \sum_{i=1}^{N} u_{ic}^{2} \| y_i - v_C \|^2 + \lambda (1 - \sum_{c=1}^{K} u_{ic}). \tag{2}$$

A solution can be obtained by alternatively computing the membership ratios u_{ic} and the centroids v_c until convergence as follows:

$$v_c = \frac{\sum_{i=1}^{N} u_{ic}^{2} y_i}{\sum_{i=1}^{N} u_{ic}^{2}}, \tag{3}$$

$$u_{ic} = \frac{1/d_{ic}}{\sum_{j=1}^{K} 1/d_{ij}}, \tag{4}$$

where $d_{ic} = \|y_i - v_C\|$.

The memberships are often initialized with random values between 0 and 1, such that the constraint of the membership is satisfied. The FCM objective function is minimized when high membership values are assigned to points whose intensities are close to the centroid of its particular class, and low membership values are assigned when a point's intensity is far from the centroid.

4 Proposed approach

The proposed method is based on a new formulation of the objective function of the standard FCM algorithm in (1) in order to incorporate *a priori* information. The new objective function is given by

$$J = \sum_{c=1}^{K} \sum_{i=1}^{N} g(v_c; \theta_c) \, u_{ic}^m \|y_i - v_c\|^2. \tag{5}$$

The functional term $g(v_c; \theta)$ models the available prior information about the class center v_c with any necessary parameters encapsulated in θ_c. A general solution of this objective function is explored in the following subsection. Then a proper form of the functional term $g(v_c; \theta_c)$ is devised in order to derive the exact formulae for the solution parameters.

4.1 Solution estimation

The objective function (5) can be minimized in a fashion similar to the standard FCM algorithm. First, a constrained minimization function using the Lagrange multiplier is constructed as

$$F = \sum_{c=1}^{K} \sum_{i=1}^{N} g(v_c; \theta_c) \, u_{ic}^m \|y_i - v_C\|^2 + \lambda \left(1 - \sum_{c=1}^{K} u_{ic}\right). \tag{6}$$

Taking the first derivatives of F with respect to u_{ic} and setting it to zero results in

$$\frac{\partial F}{\partial u_{ic}} = 0 \Rightarrow 2g(v_c; \theta_c) u_{ic} d_{ic}^2 - \lambda = 0 \tag{7}$$

Solving for u_{ic} we have

$$u_{ic} = \frac{\lambda}{2g(v_c; \theta_c) d_{ic}^2}. \tag{8}$$

Since $\sum_{j=1}^{K} u_{ij} = 1 \ \forall \ i$, then

$$\lambda = \frac{2}{\sum_{j=1}^{K} \frac{1}{g(v_j; \theta_j) d_{ij}^2}}. \tag{9}$$

Substituting (9) in (8) gives the final formula of the membership as

$$u_{ic} = \frac{\frac{1}{g(v_c; \theta_c) d_{ic}^2}}{\sum_{j=1}^{K} \frac{1}{g(v_j; \theta_j) d_{ij}^2}}. \tag{10}$$

The condition of the zero gradient of F with respect to v_c leads to

$$\frac{\partial F}{\partial v_C} = 0 \quad \Rightarrow \quad \sum_{i=1}^{N} u_{ic}^2 \left[-2(y_i - v_C) g(v_c; \theta_c) + (y_i - v_c)^2 \frac{\partial}{\partial v_c} g(v_c; \theta_c) \right] = 0. \tag{11}$$

The solution of this equation relies on the specific form of the prior information term $g(v_c; \theta_c)$ which will be devised next. Once this is done, the exact formulae to obtain the memberships and class centers can be derived.

4.2 Prior information guided solution

The class centers in the intensity domain are the central parameters that all different FCM algorithms consume most of the time in searching for their optimal values. Thus, incorporating any available information about them can guide the algorithm to find the optimal values at a reduced search time. This available information can be encapsulated in a certain distribution of the class center. If uniform distributions are assumed for all the class centers, the proposed algorithm boils down to the exact standard FCM algorithm. However, if more informative distributions can be safely assumed, the algorithm will exhibit a different behavior leading to improved results.

One may assume the typical (and often logical) Gaussian distribution of the class centers, i.e., $v_c \sim N(\mu_c, \sigma_c^2)$, where μ_c is the mean of the class center, and σ_c^2 is the variance of this center, which represents the uncertainty of our information about this center. The prior information term $g(v_c; \theta_c)$ for each class is to be taken to reflect the information about this class center distribution. One way to do this is to take it as the reciprocal of this distribution. That is,

$$g(v_c; \theta_c) = \sigma_c \sqrt{2\pi} \exp\left(\frac{(v_c - u_c)^2}{2\sigma_c^2}\right), \tag{12}$$

where $\theta_c = \{\mu_c, \sigma_c\}$ represents the class's own parameters. The intuition here behind using the reciprocal is that the more likely a class center is, the smaller the objective function (5) becomes.

Having formulated an explicit form of $g(v_c; \theta_c)$, we are ready now to draw more light on (11). Substituting from (12) in (11) and doing some manipulation will lead to a cubic polynomial in the center of each class:

$$a_3 v_c^3 + a_2 v_c^2 + a_1 v_c + a_0 = 0, \tag{13}$$

where the coefficients of this cubic polynomial are given by

$$a_3 = \sum_{i=1}^{N} u_{ic}^2,$$

$$a_2 = -\sum_{i=1}^{N} u_{ic}^2 (2y_i + \mu_c),$$

$$a_1 = \sum_{i=1}^{N} u_{ic}^2 (y_i^2 + 2\mu_c y_i + 2\sigma_c^2), \text{ and}$$

$$a_0 = -\sum_{i=1}^{N} u_{ic}^2 (2\sigma_c^2 y_i + \mu_c y_i^2).$$

The solution of the cubic polynomial (13) for each class generally gives three roots. Logically, one should consider only real roots. If, however, three such real roots are obtained, we choose the one nearest to the mean μ_c.

Now we are ready to give the complete prior-information-guided FCM (PIGFCM) algorithm, which can be summarized in the following steps:

Step 1: Set the number of the classes K and the stopping condition ε.
Step 2: Based on available prior information, set $\{\mu_c, \sigma_c\}$, $c = 1, ..., K$.
Step 3: Initialize the memberships for all points with random values between 0 and 1 such that the constraint on the memberships is satisfied.
Step 4: Set loop counter $b = 0$.
Step 5: Calculate the class center v_c, $c = 1, ..., K$, solving (13).
Step 6: Calculate the new memberships of all points in all the classes using (10).
Step 7: If max $\left| V_c^{(b)} - V_c^{(b-1)} \right| < \varepsilon$, then stop, otherwise, set $b = b + 1$ and go to Step 5. $V_c^{(b)}$ denotes the vector of all class centers v_c, $c = 1, ..., K$, obtained at iteration b.

Note that in the algorithm, the memberships are initialized randomly such that the constraint on the sum of memberships per each point is satisfied. However, other possibilities do exist. For example, the memberships of a point in all classes can start with equal values.

An even better possibility is to use the class center means from the prior information to initialize the class centers (i.e., $v_c = \mu_c$, $c = 1, ..., K$, at $b = 0$) and then use them to obtain the starting values of the memberships from (10). However, in our implementation, we follow the random initialization scenario (as exactly given in the PIGFCM algorithm outlined above) in order to make the starting point of our algorithm consistent with the standard FCM algorithm and other FCM-based methods for the sake of comparison in the experimental results section.

5 Tumor segmentation

The proposed PIGFCM algorithm segments the brain MRI volume into the main tissues. Often, the tissues related to gray matter (GM), white matter (WM), and cerebrospinal fluid (CSF), in addition to the background (BG), are the ones of interest. The user provides the prior information, $\{\mu_c, \sigma_c\}$, $c = 1, ..., K$, of these tissues based on the expertise or after analyzing sample (training) MRI datasets. Typically, the BG class center's mean and variance are assumed to be small numbers close to zero.

For pathological brain MRI, the additional class corresponding to tumor (and maybe other abnormal tissues, such as edema and necrosis) is also taken into account. The prior information about the tumor class can be gathered from tumors pre-segmented by experts from training datasets. In this work, we focus on the particular type of hyper-intense tumors (tumors that have the highest intensity among the other tissues in T1 weighted MRI), but it is easy to extend it to segment other types by incorporating information about their characteristics.

When the PIGFCM algorithm has converged, a defuzzification process takes place in order to convert the fuzzy memberships to crisp. The maximum membership procedure is typically the method employed for this purpose, assigning a point i to the class C with the highest membership: $C_i = \arg_c \max\{u_{ic}\}$, $c = 1, ..., K$.

The resulting segmented volume of the tumor class is then subjected to some post-processing in order to isolate the tumor. First, morphological operations (opening followed by hole filling) are employed to remove the isolated voxels and very small objects throughout the volume. Then a connecting component technique is applied to extract all the connected shapes in the volume. The largest component is finally presented as the desired tumor isolated from the input pathological MRI volume.

6 Experimental results

In this section, the performance of the proposed PIGFCM is evaluated for the segmentation of normal and pathological brain MRI volumes. As there are publically available standard benchmark datasets of normal synthetic and real human brain MRI volumes with known ground truth, our first series of experiments are directed to the

automatic segmentation of normal brain tissues. The proposed algorithm is first applied to 3D synthetic MRI phantoms from the BrainWeb [15]. These phantoms are T1-weighted-type MRI datasets that are realistic simulations of MRI acquisition with different levels of noise and intensity non-uniformity. They also have a ground truth volume which is used to quantify the performance of different segmentation algorithms. The algorithm is then applied to real human brain MRI volumes from the Internet Brain Segmentation Repository (IBSR) [16]. This segmentation repository provides real datasets along with their ground truth segmentation as obtained by human experts. Several experiments are conducted to demonstrate the performance of the proposed algorithm in terms of accuracy, robustness against noise, and convergence speed.

The performance of the proposed algorithm on both BrainWeb and IBSR datasets is compared with some reported fuzzy approaches: the standard FCM algorithm and the FCM algorithm with incorporated neighborhood information (NFCM) [12]. The latter algorithm is selected because it is one of the most notable FCM-based algorithms imposing spatial constraints. It is implemented and run using its best working parameters. In addition, the proposed algorithm is compared with the recent non-local FCM family of algorithms [13] (NLFCM, NL-R-FCM, and NL-Reg), and Robust Fuzzy C-means algorithm (RFCM) [39], as well as the non-fuzzy methods of expectation-maximization segmentation (EMS) [40], hidden Markov chains (HMC) [41], and statistical parametric mapping (SPM5) [42].

The second series of our experiments are carried out to evaluate the proposed algorithm performance in detecting tumors from pathological brain MRI datasets. In this case, to the best of our knowledge, there are no publically available benchmark datasets of brain MRI with tumors along with their ground truth segmentations. Thus, in order to evaluate our algorithm, we use a real MRI dataset from IBSR [16] and another from a local MRI scan center in Luxor, Egypt. The performance on these datasets is assessed by two expert radiologists from Assiut University Medical Hospital.

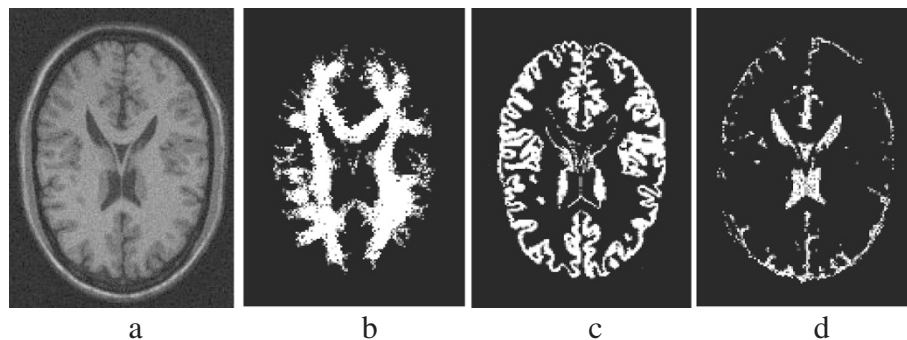## 6.1 Simulated normal MRI segmentation

Here, the brain web datasets [15] are used. Volumes in these datasets are defined at a 1-mm isotropic voxel grid, with dimensions $217 \times 181 \times 181$. The BrainWeb site provides a fuzzy tissue membership volume that represents the ground truth for each tissue class. Twenty different T1-weighted MRI volumes with noise levels ranging from 0% to 9%, and bias field from 0% to 40% are used for the experiment here. Out of those, 10 volumes are used to collect the prior information. The obtained information includes the mean μ_c and its variance σ_c of each class center. Figure 1 shows a slice of one such volume and the obtained segmentation result using the proposed algorithm.

The performance of the algorithm is assessed using two accuracy metrics: The first is the RMSE between the obtained segmentation memberships and the ground truth memberships, computed for all classes and over all the volume voxels. The second is the popular Kappa Index or (Dice similarity coefficient) [43] defined as

$$D = \frac{2|M \cap G|}{(|M| + |G|)}, \qquad (14)$$

where M refers to the segmented tissue, and G refers to the ground truth tissue. Note that the Dice metric is defined for hard memberships. Therefore, to apply it, we employ the maximum membership rule on each point's memberships as obtained from the fuzzy algorithm. The value of Dice ranges from [0,1], with 0 for no similarity, and 1 for full similarity.

The proposed algorithm is compared against a collection of algorithms, including the standard FCM, NFCM, the recent non-local FCM family of algorithms [13] (NLFCM, NL-R-FCM, and NL-Reg), and Robust Fuzzy C-means algorithm (RFCM) [39], as well as the non-fuzzy methods

Figure 1 Evaluation of the proposed algorithm on a simulated normal MRI volume. (a) One slice of a volume with 9% noise and 40% RF bias. **(b)** Segmented WM. **(c)** Segmented GM. **(d)** Segmented CSF.

Table 1 Comparison between various methods and proposed PIGFCM on the BrainWeb database

Algorithm	Noise level (%)											
	WM						GM					
	0	1	3	5	7	9	0	1	3	5	7	9
SPM5 [20]	0.91	0.95	0.95	0.93	0.90	0.86	0.91	0.94	0.93	0.92	0.88	0.85
EMS [42]	0.87	0.91	0.93	0.92	0.90	0.85	0.83	0.91	0.92	0.92	0.89	0.87
HMC [19]	0.97	0.97	0.93	0.94	0.92	0.92	0.97	0.97	0.96	0.94	0.93	0.92
FCM [11]	0.87	0.86	0.84	0.81	0.79	0.75	0.87	0.85	0.84	0.81	0.80	0.77
NFCM [12]	0.95	0.94	0.93	0.92	0.90	0.87	0.93	0.90	0.89	0.87	0.86	0.84
NL-Reg [13]	0.73	0.73	0.73	0.73	0.73	0.73	0.65	0.65	0.64	0.64	0.63	063
NL-R_FCM [13]	0.97	0.95	0.95	0.94	0.92	0.91	0.96	0.95	0.94	0.93	0.9	88
NL-FCM [13]	0.98	0.96	0.95	0.93	0.90	0.82	0.94	0.93	0.92	0.90	0.88	0.78
PIGFCM	0.98	0.98	0.97	0.95	0.94	0.93	0.96	0.95	0.94	0.92	0.90	0.87

of expectation-maximization segmentation (EMS) [40], hidden Markov chains (HMC) [41], and statistical parametric mapping (SPM5) [42]. Table 1 lists the average Dice metric on the segmented WM and GM classes for all these algorithms on the T1 BrainWeb database with 20% inhomogeneity under various noise levels.

From these results one can notice that the proposed PIGFCM algorithm has the best overall performance among all algorithms in terms of accuracy thanks to incorporating the class center prior information. This clearly shows that the proposed algorithm outperforms not only well-known fuzzy approaches, such as the standard FCM, NFCM, and NLFCM algorithms, but also key non-fuzzy approaches, such as EMS and HMC.

As previously outlined in the PIGFCM algorithm, the initialization of the class centers was done randomly thus making the starting point of our algorithm consistent with those of the standard FCM and NFCM algorithms. It is however of interest to study the effect of initialization on the three algorithms. As such, another experiment has been conducted to compare the effect of initialization on PIGFCM and the other fuzzy algorithms: standard FCM and NFCM. The average Dice and RMSE metrics over all the three brain tissues and all the test volumes for the three algorithms are tabulated in the upper part of Table 2. The three algorithms are also compared in terms of convergence speed using a pc with a 1.7-Hz P4 processor and 1-GB RAM. The running times are also given in Table 2.

From these results, one can notice that the NFCM has better results than the standard FCM algorithm. However, the proposed PIGFCM algorithm provides the best accuracy (smallest RMSE and highest Dice). Although the NFCM corrects for the effect of the MRI bias field on the segmentation accuracy [12], the proposed algorithm (which does not) provides considerably superior performance. Moreover, it has a faster trend to converge; it needs less than 0.17 of the time needed by the NFCM algorithm, and about 0.81 of the FCM algorithm. NFCM

takes rather a long time due to the more complicated calculations needed to be made at each iteration. Clearly the incorporation of the prior information about the class centers has indeed improved the segmentation accuracy of the brain tissues, and guided the algorithm to reach the proper solution faster.

The same experiment is repeated for the algorithms: FCM, NFCM, and the proposed PIGFCM after being initialized using the prior information about the class centers (i.e., $v_c = \mu_c$, $c = 1, ..., K$, at $b = 0$). Again, the segmentation accuracy and the time performance are recorded for the three algorithms; see the lower part of Table 2. One can clearly notice that the initialization has no significant effect on the accuracy, which is a good feature of the three algorithms. On the other hand, the different (and better) initialization has indeed affected the time performances positively, where the time consumed by each algorithm has dropped considerably (about three to four times of improvement).

The robustness against the noise levels is evaluated using a simulated brain MRI volume from the Brain-Web with 0% noise level and 0% bias field to produce a number of noisy volumes by adding a normal noise with zero mean and standard deviation ranging from 0 to 50. At each noise standard deviation, the three algorithms are applied and the two accuracy measures are recorded. This

Table 2 Comparison between FCM, NFCM, and PIGFCM algorithms concerning initialization

| Initialization	Algorithm	Average dice	Average RMSE	Average time (s)
Random	FCM [11]	0.86	0.115	135
	NFCM [12]	0.91	0.100	670
	PIGFCM	0.95	0.075	110
Prior information	FCM [11]	0.86	0.111	41
	NFCM [12]	0.92	0.098	221
	PIGFCM	0.97	0.060	25

is repeated 10 times for each noise standard deviation. Figure 2a graphs the average RMSE for the three algorithms, while Figure 2b plots the average Dice metric. The NFCM algorithm demonstrates somewhat better robustness against noise than FCM due to the inclusion of the neighborhood constraint that has a noise-smoothing effect. However, it is clear that the PIGFCM algorithm is the most robust among the three algorithms due to incorporating the class center priors that has a regularization effect on the algorithm output. Even at a high noise standard deviation of 50, the average RMSE of PIGFCM is only 0.8 of that of the NFCM algorithm.

6.2 Real normal MRI segmentation

The proposed algorithm is applied to 20 real MRI volumes obtained from IBSR [16] for different subjects. The volumes in these datasets are defined at a 1-mm isotropic voxel grid, with dimensions $256 \times 256 \times Z$, where Z ranges from 55 to 67 with 3.1-mm slice thickness. The ground truth segmentation of each volume as obtained by expert radiologists is also available. The prior information for each class center of the three main brain tissues is estimated from 10 volumes. The outputs of the proposed algorithm and several algorithms are assessed using the 10 remaining MRI volumes. The algorithms under
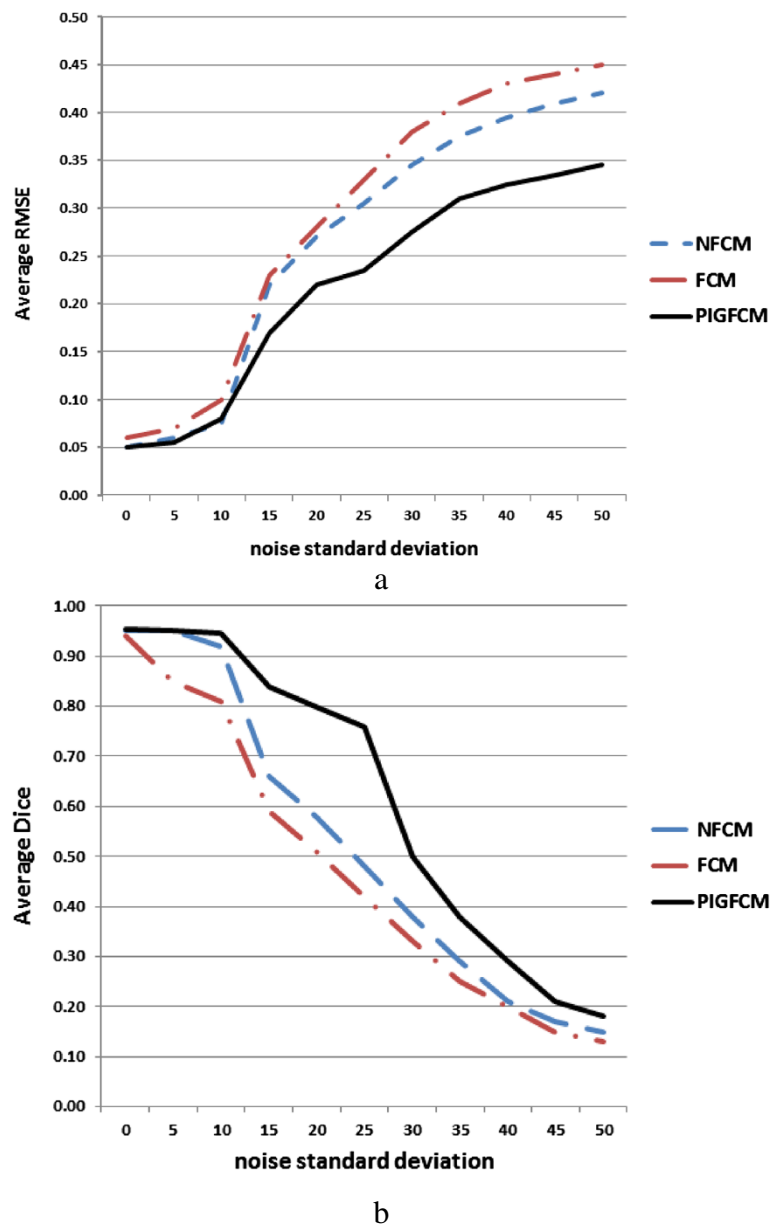
Figure 2 Accuracy of proposed (PIGFCM) algorithm and the FCM and NFCM algorithms versus noise standard deviation. (a) RMSE metric.
(b) Dice metric.
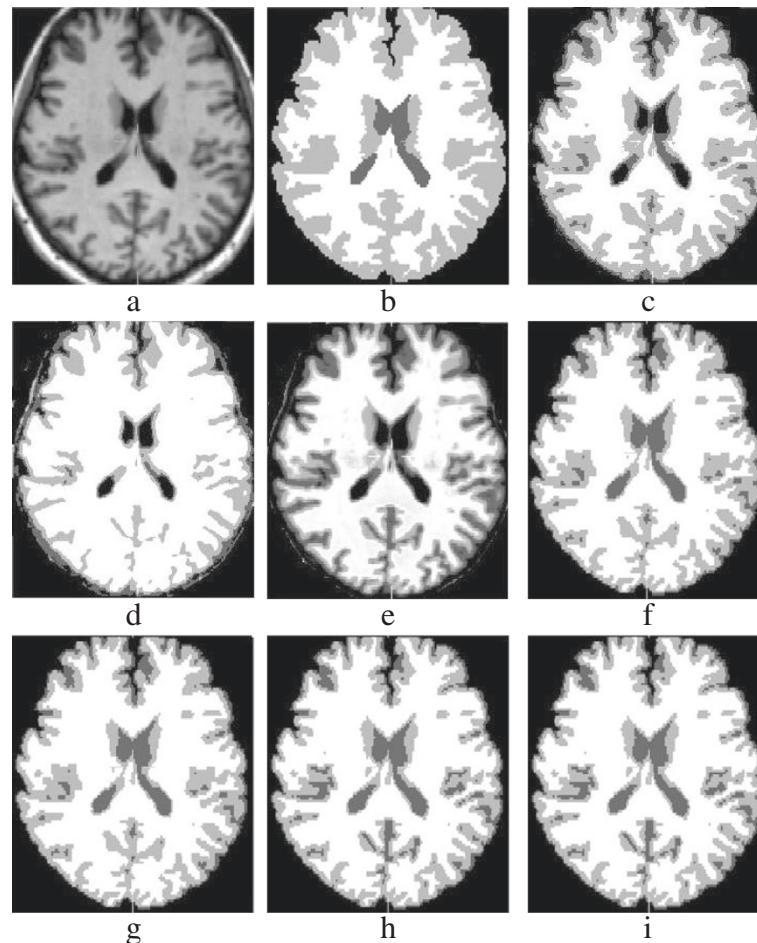
Figure 3 Results of several algorithms on the IBSR database. (a) A brain MRI slice of case 11 from IBSR. **(b)** Ground truth. Results using **(c)** PIGFCM, **(d)** NFCM [12], **(e)** FCM [11], **(f)** RFCM [41], **(g)** NL-Reg [13], **(h)** NL-FCM [13], and **(i)** NL-R-FCM [13].

comparison include the standard FCM, NFCM, the recent non-local FCM family of algorithms [13] (NLFCM, NL-R-FCM, and NL-Reg), and Robust Fuzzy C-means algorithm (RFCM) [39], as well as the non-fuzzy methods of expectation-maximization segmentation (EMS) [40], hidden Markov chains (HMC) [41] and statistical parametric mapping (SPM5) [42]. Figure 3 shows the segmentation results of the three main tissues: WM, GM, and CSF for one axial T1-weighted brain MRI slice using several of these algorithms.

The accuracy of the segmentation is assessed using the RMSE and Dice metrics. Table 3 gives the averages of the two metrics for the WM and GM tissues over the dataset volumes for the various algorithms as well as the time consumed by each algorithm. The results show that the proposed algorithm has the best overall performance among all algorithms in terms of accuracy thanks to incorporating the class center prior information. Additionally, the proposed algorithm has demonstrated the fastest performance among all algorithms. This clearly shows that

Table 3 Comparison in terms of Dice and RMSE measures and consumed times for different segmentation methods

Algorithm	Dice		RMSE		Average time (min)
	WM	**GM**	**WM**	**GM**	
HMC [19]	0.8653	0.7994	0.4013	0.4452	20
EMS [42]	0.8587	0.7894	0.3254	0.3978	21
SPM5 [20]	0.8527	0.7870	0.2832	0.2949	22
NL-R-FCM [13]	0.8435	0.8322	0.3072	0.4002	28
NL-FCM [13]	0.8468	0.7884	0.3650	0.4420	29
NL-Reg [13]	0.8631	0.8318	0.2352	0.4294	28
RFCM [41]	0.8609	0.8408	0.3823	0.4146	36
FCM [11]	0.8560	0.8321	0.2930	0.3111	4
NFCM [12]	0.8372	0.6057	0.2822	0.3742	11
PIGFCM	0.9672	0.8405	0.2442	0.2843	3

the proposed algorithm outperforms not only well-known fuzzy approaches, such as the standard FCM, NFCM, and NLFCM algorithms, but also key non-fuzzy approaches, such as EMS and HMC.

6.3 Tumor segmentation from pathological MRI

In this part of our experimental results, we evaluate the proposed approach for automatic tumor segmentation from pathological brain MRI. Assessing the performance

on such a task is not trivial due to the lack of standard benchmark datasets. Here, we test our approach on two different 3D T1-weighted datasets: (1) Tumor-Dataset-1 obtained from IBSR [16] consisting of four ($256 \times 256 \times 28$) axial scans, taken at roughly 6-month intervals over 3.5 years for a 59-year-old female at the first scan. (2) Tumor-Dataset-2 for two subjects, consisting of two axial ($256 \times 256 \times 22$) scans obtained from a local MRI scan center located in Luxor, Egypt. The two datasets exhibit

a   b   c
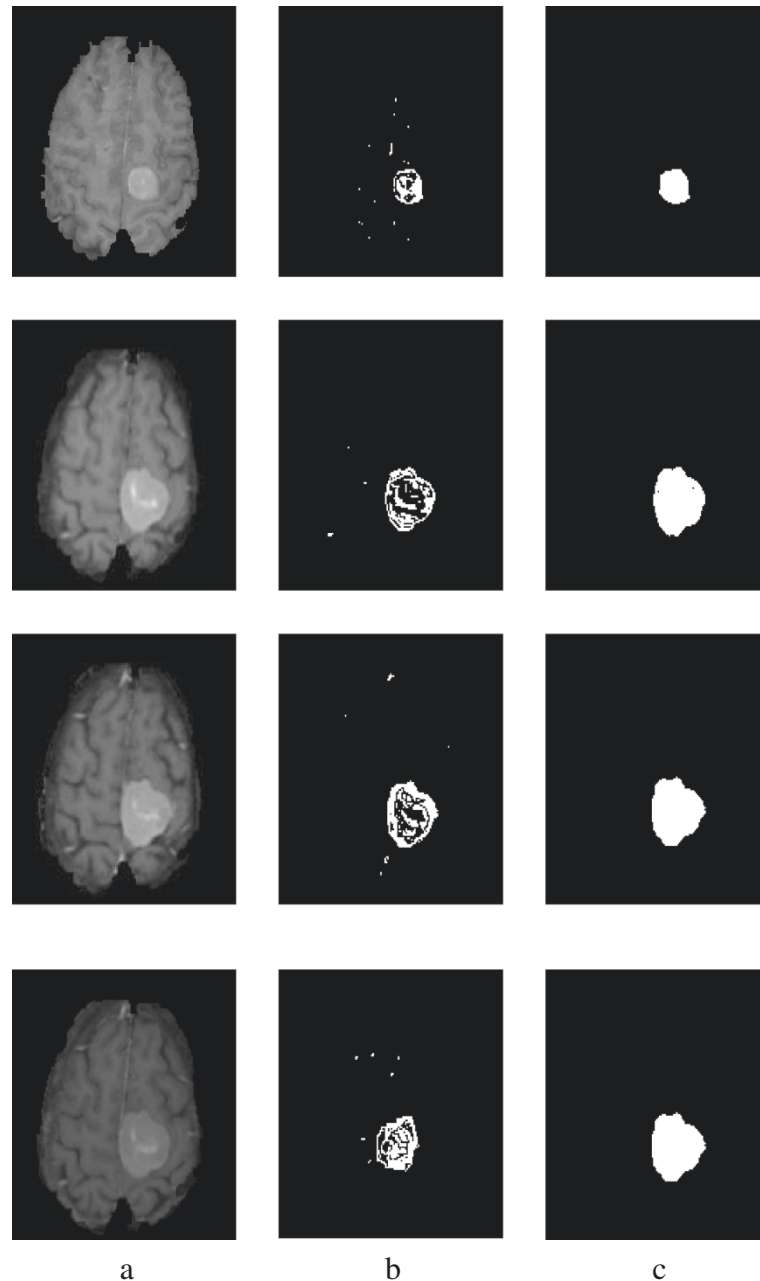
Figure 4 An example of tumor segmentation from Tumor-Dataset-1 volumes (each row shows volume at different scan time). (a) A slice of MRI volume after removing non-brain tissues such as skull. **(b)** The tumor class memberships from the PIGFCM algorithm in that slice. **(c)** The final segmented tumor after applying morphological operations.

tumors with different sizes and at different locations. For quantitative evaluation of the segmentation results; unfortunately, these datasets lack any ground truth segmentation. Therefore, we resort to two expert radiologists from Assiut University Medical Hospital to assess the algorithm outputs.

The datasets also have the skull as part of the imaged volume, so it is important to remove it in a separate pre-process. This is achieved using the Brain suite [30] automated software package for skull removing. Then the proposed approach is applied on the volumes of the datasets to segment each into the five classes (WM, GM, CSF, BG, and tumor). For all these datasets, we use the same prior information for the class centers of WM, GM, and CSF as constructed in the previous experiment using real normal IBSR datasets. The BG class center's mean and variance are assumed to be small numbers close to zero. The radiologists were independently asked to manually segment a small part of the tumor MR images of the first volume of each dataset, which is used to obtain coarse *a priori* information about the tumor class center. Figure 4 shows some slices from Tumor-Dataset-1 volumes for one subject at different scan times, along with the results of the PIGFCM algorithm. Shown on the right are the final segmented tumors after applying the post-processing morphological operations on the hardened tumor class memberships. Figure 5 illustrates analogous results on two volumes from Tumor-

Dataset-2. Both figures show good segmentations of tumors of various shapes, sizes, and locations.

All the outputs from the proposed approach are assessed by our two expert radiologists. Each radiologist was independently asked to examine each 3D output of the algorithm and assign a score out of 10. Given the limited time availability of the two radiologists, we managed to have them assess the outputs of the NFCM algorithm on all these volumes as well. The average score of the two radiologists for each volume (four volumes from Tumor-Dataset-1 and two from Tumor-Dataset-2) for the two algorithms is given in Table 4. The scores in the table surely demonstrate the high performance of the proposed algorithm as assessed by the experts. Moreover, the scores reflect its better performance over the NFCM algorithm.

7 Conclusions

In this paper, a new soft computing approach based on the fuzzy c-means algorithm is proposed for the automatic segmentation of MRI volumetric datasets. These datasets are classified to three main classes (WM, GM, CSF). The main key contribution here is that the proposed approach, for the first time in the literature, is able to utilize available prior information about the MRI tissues in the estimation process. In particular, the knowledge about the mean values of these tissues (the class centers in FCM terminology) is exploited. The uncertainty in this information is
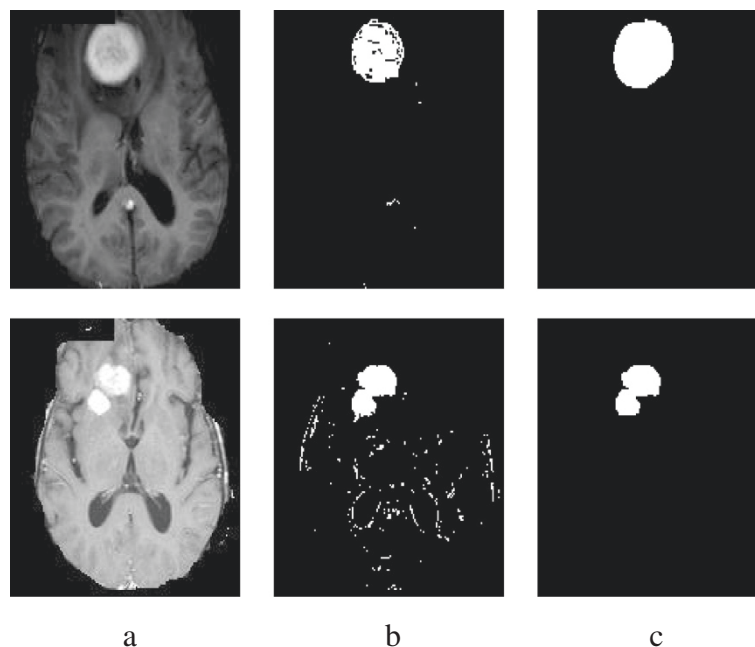
Figure 5 An example of tumor segmentation from Tumor-Dataset-2 volumes (one per row). (a) A slice of MRI volume after removing non-brain tissues such as skull. **(b)** The tumor class memberships from the PIGFCM algorithm in that slice. **(c)** The final segmented tumor after applying morphological operations.

Table 4 Average scores of two expert radiologists for outputs of PIGFCM and NFCM algorithms (out of 10)

Volume	PIGFCM	NFCM
Tumor-Dataset-1_1	9.5	9.1
Tumor-Dataset-1_2	9.0	9.0
Tumor-Dataset-1_3	9.5	8.5
Tumor-Dataset-1_4	9.8	9.0
Tumor-Dataset-2_1	8.7	8.1
Tumor-Dataset-2_2	8.5	8.0

also modeled in the proposed approach. Compared to other popular techniques for MRI segmentation, such as deformable models [6,7] and level sets [8,9], the proposed approach can automatically segment several tissues simultaneously starting from random initialization. Moreover, it deals in a straight-forward manner with the problem of partial volume effect in MRI.

We have applied the algorithm to the segmentation of several simulated and real brain normal MRI volumes. From the experimental results and the comparisons with other well-known techniques in the literature, we have shown that the incorporation of such prior information in the formulation and derivation of the standard FCM algorithm has indeed offered a considerable enhancement in the performance of the algorithm even at high degrees of noise. The new prior-information-guided FCM (PIGFCM) algorithm has resulted in not only increasing the segmentation accuracy, but also in speeding up the algorithm convergence. It does not require the tuning of any weighting factors to properly balance constraints with the data-driven objective function. In addition, the algorithm has demonstrated significant lower sensitivity to noise and non-homogeneity intensity bias. The new algorithm outperformed the performance of other fuzzy methods, such as the FCM algorithm with incorporated neighborhood information (NFCM) [12] and the non-local FCM algorithm [13], as well as other non-fuzzy methods, such as the expectation-maximization segmentation (EMS) method [40] and the hidden Markov chains (HMC) method [41].

Furthermore, we have developed an approach based on the proposed PIGFCM algorithm for the segmentation of tumors from pathological brain MRI datasets. The application of this approach on several brain T1-weighted MRI volumes with hyper-intense tumors of various sizes and different locations has demonstrated high-quality tumor segmentation as assessed by expert radiologists.

Our current research is directed to further improving the proposed algorithm by taking into account intensity non-uniformity in MRI data [5], which is often referred to as bias field. This inherent artifact in MRI is produced due to imperfection in radio frequency coil and also patient electrodynamics interactions. The bias field causes smooth variations in tissue intensities across MRI datasets. Although the bias field has little effect on visual interpretation, it may affect the accuracy of automatic processing tools, such as segmentation and registration. Therefore, reformulating the algorithm proposed here to account for bias field will further improve the MRI segmentation accuracy. In addition, the number of classes into which a given dataset is segmented is determined in the proposed algorithm in a supervised manner based on the expertise of the user (typically the radiologist). As there are a number of methods available in the literature (e.g., [44-46]) to determine this number automatically, seeking full algorithm automation, we are also investigating the employment of some of these methods in our algorithm.

Author details
[1]Electrical Engineering Department, Assiut University, Assiut 71516, Egypt.
[2]Computer and Information Systems Department, Sadat Academy, Assiut 71111, Egypt.

References
1. G Mazzara, R Velthuizen, J Pearlman, H Greenberg, H Wagner, Brain tumor target volume determination for radiation treatment planning through automated MRI segmentation. Int. J. Radiat. Oncol. Biol. Phys. **59**(1), 300–312 (2004)
2. D Weibei, S Ruan, C Yanping, D Bloyet, J Constans, A framework of fuzzy information fusion for the segmentation of brain tumor tissues on MR images. Image Vis. Comput. **25**, 164–171 (2007)
3. K Michael, K Simon, A Nabavi, M Peter, A Ferenc, R Jolesz, Automated segmentation of MRI of brain tumors. Radiology **218**, 586–591 (2001)
4. Y Zhu, H Yan, Computerized tumor boundary detection using a Hopfield neural network. IEEE Trans. Med. Imag. **16**, 55–67 (1997)
5. V Uros, P Franjo, L Bostjan, A review of methods for correction of intensity inhomogeneity in MRI. IEEE Trans. Med. Imag. **26**(3), 405–421 (2007)
6. S Luo, R Li, S Ourselin, A new deformable model using dynamic gradient vector flow and adaptive balloon forces, in *APRS Workshop on Digital Image Comp* (APRS, Brisbane, 2003), pp. 9–14
7. T McInerney, D Terzopoulos, Deformable models in medical image analysis: a survey. Med. Image Anal. **1**(2), 91–108 (1996)
8. AE Lefohn, JE Cates, RT Whitaker, Interactive, GPU-based level sets for 3D segmentation. Med. Image Comput. Computer-assisted Intervention Conference - MICCAI. Lect. Notes Comput. Sci. **2878**, 564–572 (2003)
9. S Ho, E Bullitt, G Gerig, Level set evolution with region competition: automatic 3D segmentation of brain tumors. Int. Conf. Patt. Recog. **16**(1), 532–535 (2002)
10. J Dunn, A fuzzy relative of the ISODATA process and its use in detecting compact well separated clusters. J. Cybern. **3**, 32–57 (1974)
11. J Bezdek, *Pattern Recognition with Fuzzy Objective Function Algorithms* (Plenum, New York, 1981)
12. MN Ahmed, SM Yamany, N Mohamed, AA Farag, T Moriarty, A modified fuzzy c-means algorithm for bias field estimation and segmentation of MRI data. IEEE Trans. Med. Imag. **21**(3), 193–199 (2002)
13. B Caldairou, N Passat, P Habas, C Studholme, F Rousseau, A non-local fuzzy segmentation method: application to brain MRI. Pattern Recogn. **44**(9), 1916–1927 (2011)

14. W Cai, S Chen, D Zhang, Fast and robust fuzzy c-means clustering algorithms incorporating local information for image segmentation. Pattern Recogn. **40**(3), 825–838 (2007)

15. Online simulated brain web. http://brainweb.bic.mni.mcgill.ca/brainweb/. Accessed 26 Sept 2011

16. Internet Brain Segmentation Repository (IBSR). http://www.nitrc.org/projects/ibsr. Accessed 26 Feb 2011

17. N Gordillo, E Montseny, P Sobrevilla, State of the art survey on MRI brain tumor segmentation. Mag. Resonance Imag. (31), 1426–1438 (2013)

18. P Gibbs, D Buckley, S Blackb, A Horsman, Tumour determination from MR images by morphological segmentation. Phys. Med. Biol. **41**(11), 2437–46 (1996)

19. A Stadlbauer, E Moser, S Gruber, R Buslei, C Nimsky, R Fahlbusch, O Ganslandt, Improved delineation of brain tumors: an automated method for segmentation based on pathologic changes of H-MRSI metabolites in gliomas. Neuro Imag. **23**(2), 454–461 (2004)

20. KJ Shanthi, MS Kumar, Skull stripping and automatic segmentation of brain MRI using seed growth and threshold techniques, in *the International Conference on Intelligent and Advanced Systems (ICIAS 2007)* (IEEE, Kuala Lumpur, 2007), pp. 422–426

21. Y Salman, Modified technique for volumetric brain tumor measurements. J. Biomed. Sci. Eng. **2**, 16–19 (2009)

22. W Dou, S Ruan, Y Chen, D Bloyet, J Constans, A framework of fuzzy information fusion for the segmentation of brain tumor tissues on MR images. Imag. Vision Comput. **25**, 164–171 (2007)

23. W Deng, W Xiao, H Deng, J Liu, MRI brain tumor segmentation with region growing method based on the gradients and variances along and inside of the boundary curve, in *the 3rd International Conference on Biomedical Engineering and Informatics (BMEI), vol.1* (IEEE, Yantai, 2010), pp. 393–396

24. T Tran, R Wehrens, L Buydens, Clustering multispectral images: a tutorial. Chemometrics and Intelligent Laboratory Systems, Volume 77. Issues **1–2**(28), 3–17 (2005)

25. AWC Liew, H Yan, N Law, Image segmentation based on adaptive cluster prototype estimation. IEEE Transact. Fuzzy Syst. **13**(4), 444–453 (2005)

26. S Chen, D Zhang, Robust image segmentation using FCM with spatial constraints based on new kernel-induced distance measure. IEEE Transact. Syst. Man Cybern. **34**(4), 1907–1916 (2004)

27. S Krinidis, V Chatzis, A robust fuzzy local information C-means clustering algorithm. IEEE Transact. Imag. Process. **19**(5), 1328–1337 (2010)

28. KS Chuang, HL Tzeng, S Chen, J Wu, TJ Chen, Fuzzy c-means clustering with spatial information for image segmentation. Comp. Med. Imag. Graph. **30**, 9–15 (2006)

29. M Clark, L Lawrence, D Golgof, R Velthuizen, F Murtagh, M Silbiger, Automatic tumor segmentation using knowledge-based techniques. IEEE Transact. Med. Imag. **17**(2), 187–201 (1998)

30. JY Kang, LQ Min, QX Luan, X Li, JZ Liu, Novel modified fuzzy c-means algorithm with applications. Digital Signal Process. **19**(2), 309–319 (2009)

31. F Hoppner, F Klawonn, Improved fuzzy partitions for fuzzy regression models. Int. J. Approx. Reason. **32**, 85–102 (2003)

32. L Zhu, FL Chung, S Wang, Generalized fuzzy c-means clustering algorithm with improved fuzzy partitions, IEEE Transactions on Systems, Man, and Cybernetics. Part B. Cybernetics **39**(3), 578–591 (2009)

33. Z Ji, Q Sun, D Xia, A framework with modified fast FCM for brain MR images segmentation. Pattern Recognition. **44**(5), 999–1013 (2011)

34. Y Chen, J Zhang, S Wang, Y Zheng, Brain magnetic resonance image segmentation based on an adapted non-local fuzzy c-means method. IET Comput. Vision **6**(6), 610–625 (2012)

35. K Wong, Medical image segmentation: methods and applications in functional imaging, in *Handbook Biomed Image Anal, Topics in Biomedical Engineering International Book Series* (Springer, Berlin, 2005), pp. 111–182

36. H Khotanloua, O Colliotb, J Atifc, I Blocha, 3D brain tumor segmentation in MRI using fuzzy classification, symmetry analysis and spatially constrained deformable models. Fuzzy Sets and Syst. **160**, 1457–1473 (2009)

37. G Moonis, J Liu, J Udupa, D Hackney, Estimation of tumor volume with fuzzy-connectedness segmentation of MR images. Am. J. Neuro. Radiol. **23**, 352–363 (2002)

38. J Ashburner, K Friston, Unified segmentation. Neuro Imag. **26**(3), 839–851 (2005)

39. LR Dice, Measures of the amount of ecologic association between species. Ecology **26**(3), 297–302 (1945)

40. K Leemput, F Maes, D Vandermeulen, P Suetens, Automated model-based bias field correction of MR images of the brain. IEEE Transact. Med. Imag. **18**, 885–896 (1999)

41. S Bricq, C Collet, J-P Armspach, Unifying framework for multimodal brain MRI segmentation based on hidden Markov chains. Med. Imag. Anal. **12**(6), 639–652 (2008)

42. DL Pham, Spatial models for fuzzy clustering. Comput. Vision Imag. Understanding **84**(2), 285–297 (2001)

43. D Shattuck, R Leahy, BrainSuite: an automated cortical surface identification tool. Med. Imag. Anal. **6**(2), 129–142 (2002)

44. H Sun, S Wang, Q Jiang, FCM-based model selection algorithms for determining the number of clusters. Pattern Recogn. **37**(10), 2027–2037 (2004)

45. M El-Melegy, E Zanaty, W Abd-Elhafiez, A Farag, On cluster validity indexes in fuzzy and hard clustering algorithms for image segmentation, in *IEEE International Conference on Image Processing (ICIP'07), Vol.6* (IEEE, San Antonio, TX, 2007), p. VI - 5–VI - 8

46. Y Li, Y Shen, An automatic fuzzy c-means algorithm for image segmentation. Soft Comput. **14**(2), 123–128 (2010)